

# Pilot-tone assisted 16-QAM photonic wireless bridge operating at 250 GHz

Luis Gonzalez-Guerrero, Haymen Shams, *Member, IEEE*, Irshaad Fatadin, *Senior Member, IEEE*, John Edward Wu, Martyn J. Fice, *Member, IEEE*, Mira Naftaly Alwyn J. Seeds *Fellow, IEEE*, and Cyril C. Renaud, *Senior Member, IEEE*

**Abstract**—A photonic wireless bridge operating at a carrier frequency of 250 GHz and transmitting at a data rate of 20 Gbit/s is proposed and demonstrated. To mitigate the phase noise of the free-running lasers present in such a link, the tone-assisted carrier recovery is used. Compared to the blind phase noise compensation (PNC) algorithm, this technique exhibited no penalty, and a penalty of less than 0.5 dB, when used with aggregated Lorentzian linewidths of 67 kHz and 350 kHz, respectively. The wireless bridge is also demonstrated in a wavelength division multiplexing (WDM) scenario, where 5 optical channels are generated and sent to the Tx remote antenna unit (RAU). In this configuration, the full band from 224 GHz to 294 GHz is used. Finally, to extend the data rate, two channels are digitally multiplexed at the central office (CO) forming a twin, single-sideband (SSB) signal. With this arrangement a wireless bridge of 40 Gbit/s is demonstrated.

**Index Terms**—digital signal processing, broadband communication, microwave photonics, millimeter wave communication, optical mixing, sub-THz communications, wireless bridge.

## I. INTRODUCTION

THE spectrum congestion at radio frequencies (RF) is forcing telecommunication companies to seek a solution at higher frequencies. In their 2017 technology review, Ericsson highlights the importance of the W-band (75 GHz – 110 GHz) and D-band (110 GHz – 170 GHz) for near-future fixed links [1]. In that report they also mention the possibility of using even higher frequencies in a more distant future. The reason for this is clear and can be seen in Fig. 1. The windows with relatively low atmospheric attenuation at frequencies above 275 GHz are shown by cross-hatching. Beyond this frequency the spectrum is not currently regulated. Therefore, these windows can be used entirely for data transmission, giving an unprecedented capacity in wireless communications. Included for comparison — in grey — are the windows above 100

This work was supported by the European Unions Horizon 2020 research and innovation programme under grant agreement 761579 (TERAPOD). This project has also received funding from the Engineering and Physical Sciences Research Council through the COALESCE (EP/P003990/1) grant.

L. Gonzalez-Guerrero, J. E. Wu, M. J. Fice, A. J. Seeds and C. C. Renaud are with the Department of Electronic and Electrical Engineering, University College London, Torrington Place, London, WC1E 7JE, England (e-mail: uceelgo@ucl.ac.uk; zceejew@ucl.ac.uk; m.fice@ucl.ac.uk; a.seeds@ucl.ac.uk; c.renaud@ucl.ac.uk).

H. Shams was with the Department of Electronic and Electrical Engineering, University College London, and is now with Compound Semiconductor Applications Catapult, Regus, Falcon Dr, Cardiff Bay, Cardiff CF10 4RU (e-mail: h.shams@ucl.ac.uk).

I. Fatadin and M. Naftaly are with the National Physical Laboratory, Teddington, TW11 0LW, U.K. (email: irshaad.fatadin@npl.co.uk; mira.naftaly@npl.co.uk).

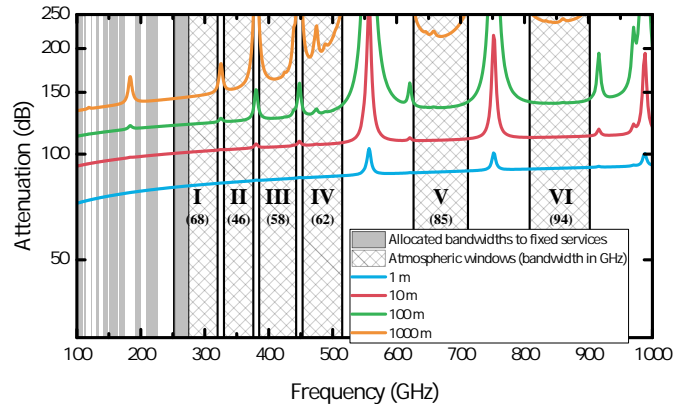


Fig. 1. Atmospheric attenuation at frequencies from 100 GHz to 1 THz. Values calculated for an atmospheric pressure of 101.300 kPa, temperature of 15°C, and a water vapor density of 7.5 g/m<sup>3</sup>

GHz currently allocated to fixed services. The widest regulated window in the W- and D-bands has a bandwidth of 12.5 GHz. As mentioned in the Ericsson report, the ultimate objective is to support data rates of 100 Gbit/s, which may be difficult with such a limited bandwidth. To achieve this capacity in an efficient way, the use of windows beyond 275 GHz will, therefore, be required. Of particular interest for long- and medium-range fixed applications (distances longer than 100 m) is the first unregulated window, which stretches from 275 GHz to approximately 320 GHz. By adding to this the 252 GHz – 275 GHz frequency range, which is already allocated to fixed services, a continuous bandwidth of 68 GHz is obtained: this is more than 5 times what is currently available in the W- and D-bands. In the research community, communications using these frequencies are commonly referred to as sub-THz wireless communications.

Among the applications envisaged for sub-THz communications, wireless bridges have attracted significant interest [2], [3]. Wireless bridges refer to wireless links connecting two portions of a fibered network. Unlike in mobile fronthaul or backhaul links, in these links the signal is not demodulated in the receiver antenna unit, but rather up-converted to the optical domain and transmitted to an optical receiver through an extra portion of fiber. This application is unique to this part of the spectrum in the sense that it is the only region with potential to achieve wireless data rates comparable to those found in optical networks or, at least, the access part of such networks. It is obvious that a seamless integration

of the wireless transmitter with the optical fiber network is an important requirement of wireless bridges. In this regard, photonic generation of THz signals offers a significant advantage over electronic generation as it directly maps the optical signal to the THz domain [4], [5]. Electronic approaches, on the other hand, need to downconvert the optical signal before THz generation.

In this paper we demonstrate a photonic wireless bridge operating at 250 GHz and using a carrier recovery scheme based on the transmission of a reference pilot tone. Compared to our previous work in [6] there are two fundamental differences: the first one is that envelope detection is no longer used for demodulation, and the second that the transmission reported here incorporates the second portion of optical fiber (after THz reception) that characterizes wireless bridges.

The rest of the paper is organized as follows. Section 2 provides a review of the various configurations that a photonic wireless bridge can adopt together with notable transmission results published in the literature. In section 3, the digital signal processing (DSP) employed throughout this paper and the experimental arrangement used for transmission are explained. Section 4 discusses the results obtained for a single-channel THz bridge operating at 250 GHz and transmitting 5 Gbd 16-quadrature amplitude modulation (QAM) signals (i.e., gross data rate of 20 Gbit/s). In this section, the results for the proposed carrier recovery technique and two different aggregated linewidths are discussed and compared with those obtained with a state-of-the-art phase noise compensation algorithm. In section 5, the proposed wireless bridge is demonstrated in the context of a wavelength division multiplexing (WDM) network scenario. In this section, a wireless bridge using the full spectrum from 224 GHz to 294 GHz is realized. In section 6, two wireless channels are digitally multiplexed and transmitted simultaneously achieving a net data rate of 40 Gbit/s. Finally, in section 7, the manuscript is summarized highlighting its main contributions.

## II. THZ WIRELESS BRIDGES

Fig. 2 (a) presents a depiction of a THz wireless bridge based on photonic THz generation. Fig. 2 (b) presents the various methods for THz-to-optical conversion (note that only schemes supporting higher-order modulation are considered) that can be used at the receiver remote antenna unit (Rx RAU). The simplest one is the direct mapping of the incoming THz field to the optical domain via an ultrawide bandwidth optical modulator. Recently, several demonstrations of this concept using plasmonic modulators (which can exhibit remarkably high electrical bandwidths [7]) have been reported [3], [8]. After optical mapping, an optical filter is needed to select one of the data-carrying sidebands. However, since the wavelength separation between carrier and sideband will be at least a couple of nm if the transmission is as THz frequencies, a narrow-bandwidth optical band pass filter (OBPF) is not required.

The alternative approach is to down-convert the THz signal first and then perform the up-conversion to the optical domain via a conventional optical modulator. For THz downconversion

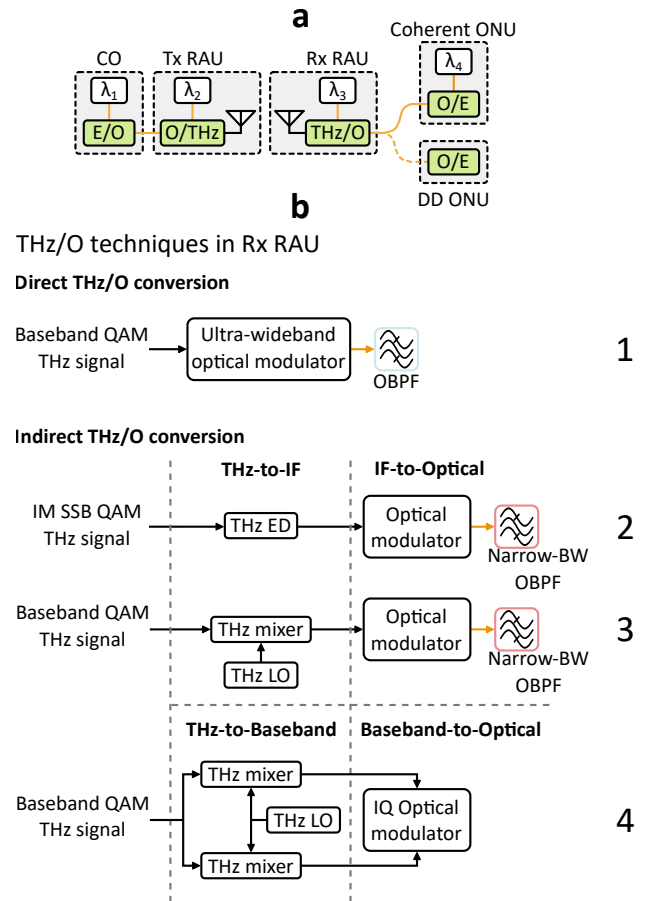


Fig. 2. (a) schematic representation of a wireless bridge based on photonic THz generation and (b) methods for THz-to-optical conversion in the Rx RAU (only schemes supporting higher-order modulation are considered). Note that only schemes 2 and 3 are compatible with a direct detection (DD) optical network unit (ONU). For schemes 1 and 4, a coherent optical receiver must be employed to recover the signal. CO: central office; OBPF: optical band-pass filter; IM: intensity modulated; SSB: single sideband; QAM: quadrature amplitude modulation; ED: envelope detector.

either homodyne [2], heterodyne [9], [10], or direct [11] detection can be used. The advantage of the homodyne receiver is that no redundant signal is generated and, hence, it does not require a narrow-bandwidth optical band-pass filter (OBPF) to remove it. On the other hand, down-conversion to an intermediate frequency (IF), either with an envelope detector (ED) or heterodyne receiver, simplifies the number of high-frequency components in the receiver RAU, making it a more cost-effective solution.

In Table I, relevant experiments on wireless bridges supporting higher order modulation formats are summarized. For the sake of comparison only transmissions achieving bit error rates (BERs) below the hard-decision forward error correction (HD-FEC) limit of  $3.8 \times 10^{-3}$  are shown. The highest data rate fulfilling this condition so far is 80 Gbit/s, achieved using polarization multiplexing (PM) and 16-QAM modulation. However, this was obtained in a system operating at a carrier frequency below 100 GHz [12]. Above 100 GHz, systems supporting only quadrature phase shift keying (QPSK) in either single carrier or multi-carrier (i.e., orthogonal frequency division multiplexing, OFDM) modulation formats have been

TABLE I  
WIRELESS BRIDGES SUPPORTING HIGHER-ORDER MODULATION

| Frequency (GHz) | Gross data rate (Gbit/s); Format | Wireless distance (cm) | THz emitter | THz amplifier | Optical distance (km) | THz/O technique | ONU      | Reference |
|-----------------|----------------------------------|------------------------|-------------|---------------|-----------------------|-----------------|----------|-----------|
| 95              | 80; PM-16QAM                     | 100                    | Photonic    | Tx & Rx       | 100                   | 2               | Coherent | [12]      |
| 20              | 9; OFDM QPSK                     | 50                     | Electronic  | Tx & Rx       | 40                    | 2               | DD       | [13]      |
| 60              | 10/20; QPSK                      | 500/100                | Photonic    | Tx            | -                     | 1               | Coherent | [3]       |
| 288.5           | 36; QPSK                         | 1600                   | Photonic    | Rx            | -                     | 1               | Coherent | [8]       |
| 300             | 40; QPSK                         | 10                     | Photonic    | Rx            | 10.5                  | 2               | Coherent | [10]      |
| 450             | 13; QPSK                         | 380                    | Photonic    | -             | 12.2                  | 2               | DD       | [9]       |

demonstrated so far. The realization of a wireless bridge at sub-THz frequencies with a more efficient format is, thus, a pending task. This, however, may prove challenging given the number of free-running lasers associated with this type of link. As shown in Fig. 2 (a), this figure can go up to 4 if a coherent optical network unit (ONU) is used at the optical receiver.

To enable the use of both cost-efficient foundry-fabricated lasers and spectrally-efficient modulation formats (i.e., without incurring on a high penalty), a robust phase noise compensation technique is essential in this type of link. One possible solution is to use the configuration number 2 in Fig. 2 with the envelope detector (ED). As demonstrated in [6], this scheme is insensitive to phase noise. However, this approach would only compensate the phase noise from the CO and Tx RAU lasers. Furthermore, the increased sensitivity of heterodyne receivers, compared to that of EDs [5], may be crucial to achieve reasonable wireless transmission distances. To keep the phase noise tolerance associated with envelope detection while using heterodyne down-conversion, the pilot tone-assisted technique may be used [14]. The basic idea behind this technique is to transmit a pilot tone together with the data-carrying signal in order to track the symbol deviations introduced by phase noise. In the ONU, after signal digitization, this tone is used to coherently down-convert the signal.

### III. DSP AND EXPERIMENTAL ARRANGEMENT

In this paper the pilot tone and the signal are generated via the single sideband-with carrier (SSB-C) modulation format, which is implemented via an IQ modulator and a digital Hilbert transform (see Fig. 3 (a)) [6]. The pilot tone-to-signal power ratio (PTSPR), whose optimum value depends on the amount of noise present in the system, is set by adjusting the IQ modulator bias. For low PTSPRs, the modulator is biased close to null; for high PTSPRs, on the other hand, the biasing points are set close to quadrature.

The carrier recovery approach implemented in this work combines the tone assisted technique (see Fig. 3 (b)) and the square QAM-adapted Viterbi-Viterbi (VV) algorithm [15]. The former is used for frequency offset estimation (FOE) and phase noise compensation (PNC). The latter, on the other hand, is only used to compensate a fixed phase offset (a very large averaging block is used). The fixed phase offset results from the biasing points of the I- and Q-components in the optical IQ modulator as detailed in [16]. In a practical system, this offset may be removed with a single-phase rotation without

the Viterbi-Viterbi algorithm to reduce digital complexity [17]. Here, since we were constantly changing the modulator biasing points to adjust the PTSPR, the Viterbi-Viterbi algorithm was used to avoid measuring the phase offset at each PTSPR value. The receiver DSP, apart from carrier recovery, includes matched filtering and radius-directed and decision-directed equalization.

The complete experimental arrangement used in the transmissions is shown in Fig. 4. For digital signal generation, four  $2^{11}$  de Bruijn bit sequences were mapped into the 5 GBd 16-QAM symbols using Matlab. For SSB-C signal generation, after applying a root raised cosine (RRC) filter with a roll-off factor of 0.1, the signal was up-converted to a frequency of 3.25 GHz, giving a guard band (GB) between tone and signal of 500 MHz and a total passband bandwidth of 6 GHz. The resultant waveforms after applying the transmitter DSP were uploaded to an arbitrary waveform generator (AWG) operating at 50 GSa/s. The two signals generated in the AWG were time-aligned with two phase shifters and electronically amplified before being fed to the optical modulator. At the CO, an external cavity laser (ECL#1) emitting at a wavelength of 1551 nm was used for data modulation. A single mode fiber (SMF) with a length of 10 km was used to connect the CO to the Tx RAU. The optical signal received at this unit was combined with an optical tone at a wavelength of 1549 nm (giving a frequency separation between the two optical signals of around 250 GHz) from ECL#2, which was also used for the Rx RAU to simplify the system. After optical amplification and filtering, the two optical tones were fed into an unpackaged uni-travelling carrier photodiode (UTC-PD) by means of a lensed fiber. Horn antennas with a gain of 25 dBi were used for both transmission and reception and placed at 0.24 m from each other. A pair of Teflon lenses with a 5 cm diameter and a back focal length of 63.2 mm were

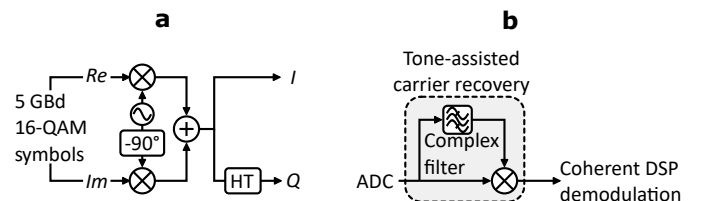


Fig. 3. (a) Tx DSP for the generation of SSB-SC signals and (b) Rx DSP for carrier recovery through the tone-assisted technique.

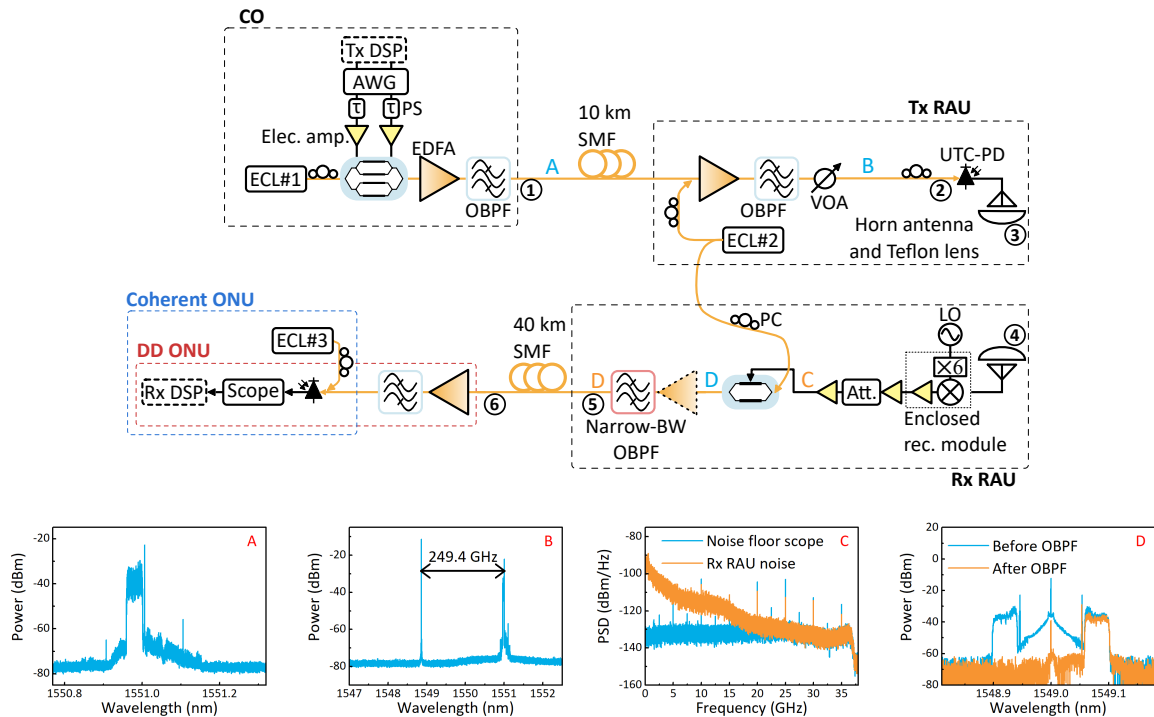


Fig. 4. Complete experimental arrangement. The numbers throughout the link denote the points at which the signal-to-noise ratio (SNR) was measured (see Fig. 5 (B)). The dashed amplifier at the Rx RAU was only used with the coherent ONU. For the DD ONU, this amplifier was placed at the receiver unit. Insets: (A) optical spectrum of the SSB signal generated at the CO; (B) spectrum at the input of the UTC-PD; (C) electrical noise at the Rx RAU (this was measured connecting the output of the 3rd IF amplifier directly to the real-time scope when no THz signal was transmitted); (D) optical spectrum of the signal generated in the Rx RAU before (blue trace) and after (orange trace) the OBPF.

inserted between the two antennas (separation between lenses was around 10 cm) to increase the collimation of the THz beam. Such lens diameter gives a theoretical maximum gain of around 42 dB — according to  $G = (4\pi S)/\lambda^2$  where  $G$  is the gain,  $S$  is the area of the lens, and  $\lambda$  is the wavelength of the electromagnetic wave and corresponding to the diffraction-limited lossless case [18] — which results in a total 84 dB gain for the two lens-antenna pairs. Note, however, that, due to the short transmission distance used in the experiment, a link budget calculation using the Friis formula would give unrealistic results [19].

On the Rx RAU, the signal was down-converted to a frequency of around 9 GHz with an enclosed receiver module (WR3.4MixAMC from Virginia Diodes) consisting of a  $\times 6$  multiplier, a second harmonic mixer (SHM), and an IF amplifier. After down-conversion, the IF signal was passed through two additional IF amplifiers. The resultant electrical signal was used to drive an intensity modulator (IM) which, depending on the optical receiver used, was biased either at the null point (for coherent ONU) or close to quadrature (for DD ONU). After optical amplification, the signal from the IM was filtered with a narrowband OBPF to suppress the upper sideband. Finally, after propagation through 40 km of SMF, the signal was detected and digitized in the ONU. This unit consisted of a single-ended PD, an 80 GSa/s real-time oscilloscope (analog bandwidth of 36 GHz) and (a) an ECL (ECL#3) in the case of coherent reception or (b) an EDFA and a 1 nm OBPF in the case of direct detection. Signals of 10  $\mu$ s of duration (giving a total number of bits of around  $2 \times 10^5$ )

were used for bit error counting.

In Fig 5 (A) the IF response of the Rx RAU (SHM, IF amplifiers and modulator) is shown. As can be seen, the IF response has a notable roll-off at low frequencies. This is mainly associated with the frequency response of the 2nd IF amp, which exhibits a roll-off close to DC. In spite of this, the overall response still exhibits a sufficiently wide region (bandwidth  $> 9$  GHz) with low power variations (maximum variation of less than 5 dB) to accommodate the 5 Gbd signals. The response drop beyond 14 GHz is due to the limited bandwidth of the 3rd IF amp., which has a 3-dB bandwidth specification of 12 GHz.

To see the signal degradation throughout the link, SNR measurements were taken in the points specified in Fig. 4 with numbered circles. The SNR was calculated as  $E[|X|^2]/E[|Y - X|^2]$ , where  $X$  and  $Y$  are the transmitted and received symbols, respectively. As can be seen from Fig. 5 (B), there is a slight drop in SNR around 1.3 dB when increasing the wireless distance by inserting the two Teflon lenses. On the other hand, a gain of more than 3 dB is achieved by employing the coherent receiver at the ONU. In the rest of the paper, the coherent ONU is always used.

#### IV. PHASE NOISE TOLERANCE

In the first instance, BER measurements were taken with the experimental arrangement shown in Fig. 4 for varying optical power injected to the UTC-PD. To see the penalty associated with higher-linewidth lasers, ECL#2 was replaced by a distributed feedback (DFB) laser in the Rx RAU. For both

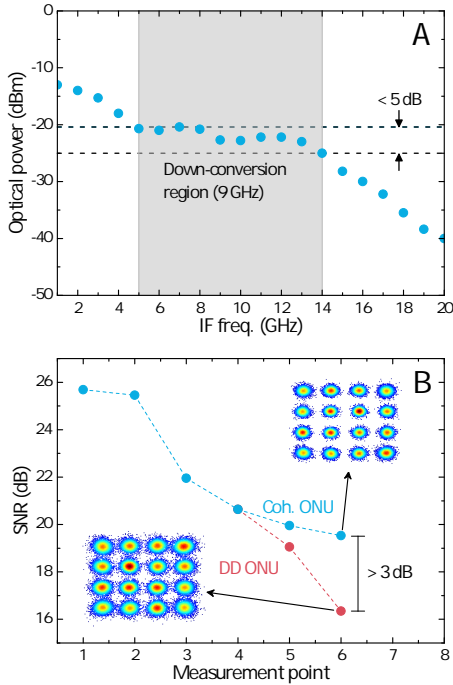


Fig. 5. (A) IF response of the Rx RAU. For the measurement, the output of the IM (biased at null) was connected to an optical spectrum analyzer, where the power of the low-frequency sideband was measured. The THz frequency was kept fixed and the RF LO was tuned to scan the downconversion frequency. (B) SNR degradation throughout the wireless bridge. The measurements points are highlighted in Fig. 4. For point 3, the transmitter and receiver antennas were placed very close (around 1 cm separation) with no lenses in between. From point 3 onwards, measurements were taken at a constant photocurrent of around 2.15 mA.

lasers, the frequency modulation (FM) noise spectrum of the 10  $\mu\text{s}$  signal received at the ONU (i.e., including all sources of phase noise throughout the link) was measured when no data was being transmitted. The received tone was digitized and processed digitally offline (down-converted, filtered and resampled) before estimating the white frequency noise component and the Lorentzian linewidth [20]. In Fig 6, the FM noise spectrum for each arrangement is shown. Linewidths of 70 kHz and 359 kHz were estimated when using ECL#2 and the DFB laser, respectively, at the Rx RAU.

To provide a reference for comparison, transmission experiments were also carried out using the blind PNC technique

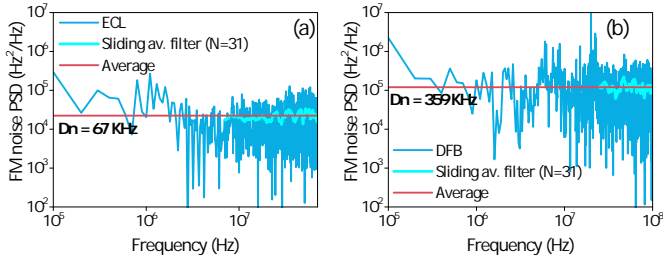


Fig. 6. FM noise spectrum of the received tone at the ONU when using, at the Tx RAU, (a) ECL#2 and (b) the DFB laser. The cyan curve shows the white region of the FM noise after being passed through a sliding averaging filter with 31 taps. The red curve is the average of the filter output (which is then multiplied by  $\pi$  to calculate the Lorentzian linewidth).

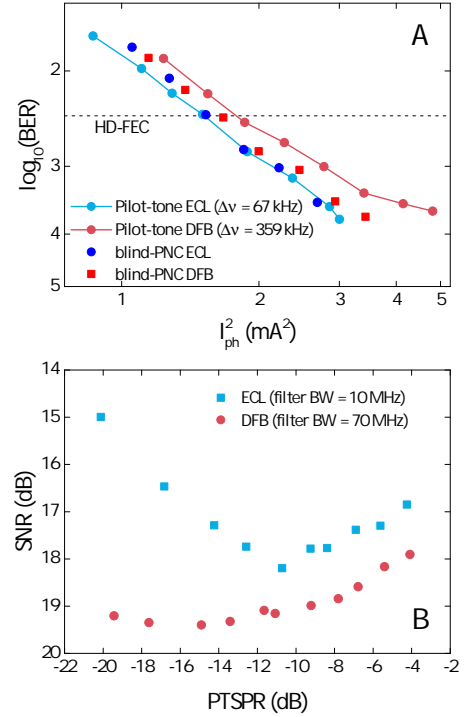


Fig. 7. (A) BER curves for various transmission arrangements, and (B) SNR against PTSPR for ECL#1 (red circles) and the DFB laser (blue squares) — the optimum filter bandwidth for each case is stated in the caption.

described in [21]. This algorithm has been reported to achieve “nearly optimum linewidth tolerance” [22] and, thus, is a good reference for comparison. The disadvantage of this algorithm, on the other hand, is its high implementation complexity, which arises from the high number of test phases required to produce an accurate estimation. In our case, 32 test phases were employed, as this is the lowest number that achieves optimum performance for 16 QAM. When using this algorithm, the IQ optical modulator at the CO was biased at null as no reference pilot was needed. Note that, apart from the intrinsic complexity of the PNC algorithm, a separate FOE algorithm is required when using this approach (unlike in the pilot tone-assisted technique). Here, a fast Fourier transform (FFT)-based algorithm was employed for FOE [23].

In Fig. 7 (A), the BER curves for all transmission configurations are shown against the UTC photocurrent squared (proportional to the generated THz power). A penalty of less than 1 dB was found when switching from ECL#2 to the DFB laser while using the pilot-tone assisted technique. The reason for this penalty is related to the PTSPR, which depends on the amount of FM noise in the system. For low levels, a narrow digital filter can be used to select the tone, minimizing the amount of additive white Gaussian noise (AWGN). This enables the use of low PTSPRs and, hence, biasing the IQ modulator closer to null, where the power — and, thus, the SNR — of the data-carrying sideband is maximized. On the other hand, as the linewidth broadens, a wider filter is needed to correctly track the faster phase distortions. This increases the level of AWGN. To compensate for this and achieve a decent SNR in the filtered tone, the PTSPR must be increased.

This, however, compromises the SNR of the signal as less power is allocated to it. In Fig. 7 (B), the SNR versus the PTSPR is plotted for ECL#2 and the DFB laser. The optimum PTSPR was found to be -15 dBm and -11 dBm, for the DFB laser and ECL#2, respectively. These values were used in the BER curves shown in Fig. 7 (A).

On the other hand, the blind PNC technique exhibits about half the penalty for the DFB with pilot when the linewidth is increased to 359 kHz. This agrees with the results presented in [21], where a small penalty ( $< 0.5$  dB) is found when going from a linewidth-times-symbol-duration product of  $1.410^{-5}$  (ECL#2) to  $7.510^{-5}$  (DFB laser) in 16-QAM (see Fig. 7 of [21]). Regarding the comparison between the two PNC schemes, no difference between them is found when using ECL#2 and a small penalty (around 0.5 dB) when using the DFB laser. The tone-assisted technique, hence, seems a good candidate for practical systems due to its simplicity (it only requires a band pass filter and a multiplication as noted in Fig. 3 and also removes the need for FOE).

## V. WIRELESS BRIDGE ON A WDM NETWORK

In reality, the wireless bridge is likely to be part of a multiuser network where a single CO serves several ONUs by means of wavelength division multiplexing (WDM). To demonstrate this type of scenario, a 5-optical channel CO was built and integrated with the wireless bridge as shown in Fig. 8. In the Tx RAU, a narrow OBPF was then used to de-multiplex one channel at a time. Keeping the wavelength of the Tx RAU optical LO fixed for all 5 channels, the full spectrum from 224 GHz to 294 GHz was used.

In Fig. 8, the experimental arrangement used for optical channel generation is shown. As can be seen, an optical frequency comb generator (OFCG) followed by a narrow-band OBPF was used to generate the 5 optical lines. The line separation was set to around 17.4 GHz, which was close to the maximum supported by the OFCG — limited by the bandwidth of the electrical driver amplifiers — and chosen to minimize the channel cross-talk introduced by the decorrelation unit. This unit was composed of a wavelength selective switch (WSS) and a fiber propagation stage with a physical length mismatch between the odd and even branches of 4 m (corresponding to around 90 symbols).

In Fig. 9 (A), the BER curve of each channel is plotted against the squared photocurrent. To quantify the penalty associated with the multi-channel operation, the BER curve of a single channel was also measured. In this case, the 2nd narrow OBPF in Fig. 8 was placed immediately after EDFA#3 (i.e., before the 10 km of SMF) so that only one channel propagated through the fiber. EDFA#3 was operated, in this case, at maximum output power, which was measured to be 14.5 dBm. For the 5-channel transmission, on the other hand, the optimum output power from EDFA#3 was found to be around 7.5 dBm. A penalty of less than 2 dB at the FEC limit was found between the single- and multiple-channel transmissions. The penalty of each channel with respect to the 241.57 GHz channel (in multiple-channel operation) is plotted in Fig. 9 (B). The THz response of the system (UTC-PD and

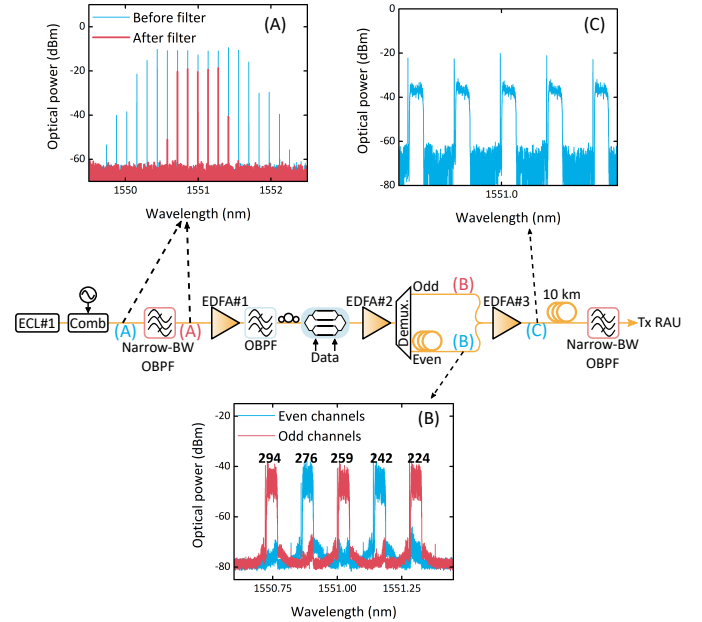


Fig. 8. Experimental arrangement for generation of multiple optical channels at the CO. The optical comb is generated with a dual-drive Mach-Zehnder modulator (DD-MZM) as detailed in [24]. Inset (A) shows the comb lines before (blue trace) and after (red trace) optical filtering. Inset (B) shows the even (blue trace) and odd (red trace) channels before being recombined (in the moment of capturing the spectrum, the IQ modulator was biased close to null). The black label indicates the wireless frequency, in GHz, of each channel during the transmission experiments. Inset (C) displays all the channels and their pilot tones after EDFA#3.

SHM) is also shown in this figure. As can be seen, there is a strong correlation between the two curves: the higher penalty of the high-frequency channels is likely to be due to the system response roll-off at higher frequencies.

## VI. 40 GBIT/S WIRELESS BRIDGE

To increase the data rate, two 5 GBd 16-QAM channels were digitally multiplexed in the digital domain using a technique called twin-SSB. The basic idea behind this technique is to generate two digital SSB signals and, through appropriate DSP (see Fig. 10), map them to opposite sidebands. At the receiver, the pilot tone is used to downconvert both signals. Using ECL#2 at the Rx RAU, a twin-SSB signal with a total passband bandwidth of 11.25 GHz (in this case, based on the required filter bandwidths found in section IV, the upconversion frequency was reduced to 2.875 GHz) was generated and transmitted through the wireless bridge. The spectrum of both the optical signal generated at the CO and the received signal at the ONU are shown in Fig. 11 (A) and (B), respectively. Note that the downconversion frequency shown in Fig. 11 (B) (i.e., around 25 GHz) is the downconversion frequency employed at the ONU and corresponds to the frequency difference between ECL#3 and the optical signal generated at the Rx RAU. The THz downconversion frequency, on the other hand, corresponds to the difference between the pilot tone and the tone located at around 15 GHz, which is the suppressed carrier of ECL#2.

In Fig. 11 (C), the BER of each channel as well as the total BER is plotted versus the squared UTC photocurrent.

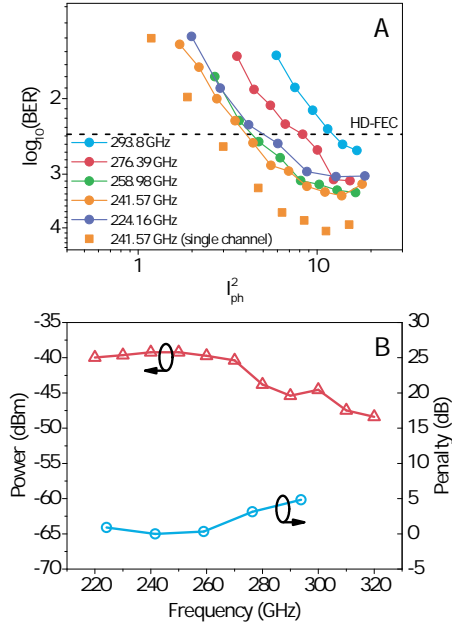


Fig. 9. (A) BER vs. squared photocurrent for each channel in the multiple-channel configuration and also the 241.57 GHz channel in the single-channel configuration and (B) THz response of the system and penalty of each channel. The THz frequency was scanned by tuning ECL#2. The response was measured by connecting the enclosed receiver directly to an electrical spectrum analyzer. The RF LO frequency was also tuned to ensure downconversion to the same IF (10 GHz).

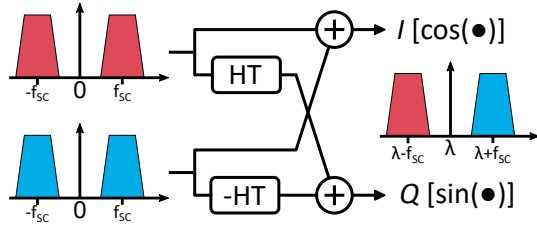


Fig. 10. DSP employed to generate the twin-SSB signal

Ch. 1, which is the channel that was downconverted to lower IF frequencies in the Rx RAU (see Fig. 11 (B)), exhibits some penalty with respect to Ch. 2. This is because, at low IF frequencies, although the system response is higher (see Fig. 5 (A)), there is more electrical noise (see Fig. 4 inset (C)). In fact, we found that, when downconverting to very low IF frequencies, the signal quality was degraded quite substantially (the signal just became buried under the noise).

From the BER curve and the constellation diagrams in Fig. 11 (C) it is easy to see that the signal suffers from compression effects for photocurrents higher than 3 mA. Since neither changing the amplifiers nor increasing the degree of attenuation after the enclosed THz receiver corrected this (i.e., saturation effects occurred at the same value of photocurrent), these effects are likely to be caused by the THz receiver itself. Connecting directly the receiver to an electrical spectrum analyzer (ESA) and with no modulation being sent, a power of around -40 dBm was measured for a photocurrent of 3 mA. Taking into account the power losses from the receiver, cable, and ESA, this power translates into around -30 dBm

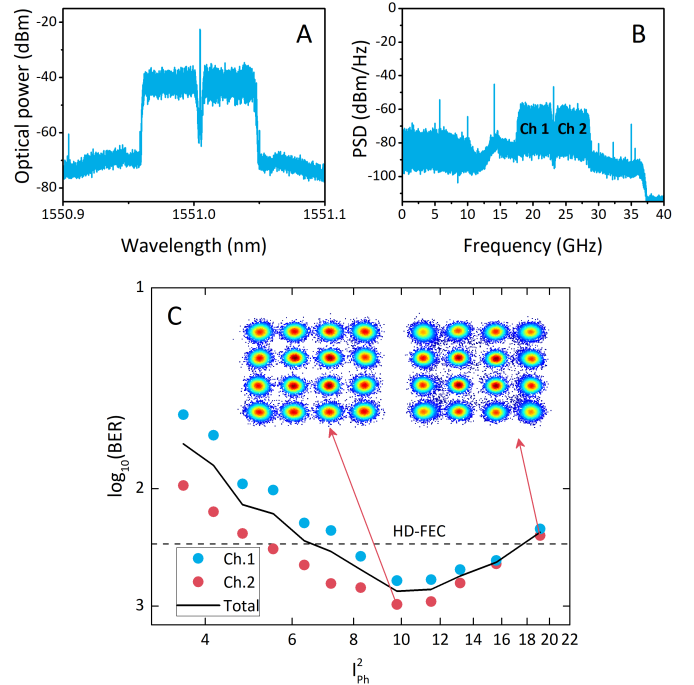


Fig. 11. (A) Optical spectrum of the twin-SSB signal; (B) electrical spectrum of the received twin-SSB signal at the ONU; (C) BER vs. squared photocurrent for each of the sub-channels and the total BER. The insets in (C) show the constellation diagrams of Ch. 2 at the minimum-BER and maximum-photocurrent points.

of received THz power. It is important to mention that the saturation point when transmitting a QAM signal (i.e., without the pilot tone) was higher. This is likely to be due to the higher peak-to-average power ratio (PAPR) of the twin-SSB signal.

## VII. CONCLUSION

The wide transmission bandwidths found at sub-THz frequencies make this part of the spectrum a strong candidate for ultra-fast wireless communications. Among the envisaged applications of sub-THz communications, wireless bridges have attracted significant interest due to the wide range of scenarios where they may be used. Due to their high integration potential with optical networks, THz wireless bridges based on photonic technologies offer a clear advantage over the electronic counterpart. In this paper, a photonic wireless bridge operating at 250 GHz and transmitting 20 Gbit/s is proposed and demonstrated. First, the performance of a coherent optical receiver (at the ONU) is compared to that of a DD receiver via SNR measurements. A gain higher than 3 dB is found when using coherent detection, confirming its superior performance. In order to mitigate the phase noise of the 4 free-running lasers present in such a link the tone-assisted carrier recovery is used. No penalty, and a penalty of less than 0.5 dB with respect to the blind PNC algorithm are found when using this technique with aggregated Lorentzian linewidths of 67 kHz and 359 kHz, respectively, and 5 GBd 16-QAM signals. Based on these results and its simplicity, this algorithm may be a good candidate for this type of links. The wireless bridge is also demonstrated in a WDM scenario, where 5 optical channels

are generated and sent to the Tx RAU. In this unit, one channel is selected at a time and transmitted wirelessly. With this configuration, the full band from 224 GHz to 294 GHz is used. Finally, to extend the data rate, two channels are digitally multiplexed at the CO forming a twin-SSB signal. With this arrangement a wireless bridge of 40 Gbit/s is demonstrated.

## REFERENCES

- [1] J. Edstam, J. Hansryd, S. Carpenter, T. Emanuelsson, Y. Li, and H. Zirath, "Microwave backhaul evolution-reaching beyond 100GHz," *Tech. Rep.*, 2017.
- [2] S. Koenig, D. Lopez-Diaz, J. Antes, F. Boes, R. Henneberger, A. Leuther, A. Tessmann, R. Schmogrow, D. Hillerkuss, R. Palmer, T. Zwick, C. Koos, W. Freude, O. Ambacher, J. Leuthold, and I. Kallfass, "Wireless sub-THz communication system with high data rate," *Nature Photonics*, vol. 7, no. 12, pp. 977–981, 2013.
- [3] Y. Salamin, B. Baeuerle, W. Heni, F. C. Abrecht, A. Josten, Y. Fedoryshyn, C. Haffner, R. Bonjour, T. Watanabe, M. Burla, D. L. Elder, L. R. Dalton, and J. Leuthold, "Microwave plasmonic mixer in a transparent fibreless link," *Nature Photonics*, no. Mim, 2018. [Online]. Available: <http://www.nature.com/articles/s41566-018-0281-6>
- [4] A. J. Seeds, H. Shams, M. J. Fice, and C. C. Renaud, "TeraHertz photonics for wireless communications," *Journal of Lightwave Technology*, vol. 33, no. 3, pp. 579–587, 2015.
- [5] T. Nagatsuma, S. Horiguchi, Y. Minamikata, Y. Yoshimizu, S. Hisatake, S. Kuwano, N. Yoshimoto, J. Terada, and H. Takahashi, "Terahertz wireless communications based on photonics technologies," *Optics Express*, vol. 21, no. 20, p. 23736, 2013. [Online]. Available: <https://www.osapublishing.org/oe/abstract.cfm?uri=oe-21-20-23736>
- [6] L. Gonzalez-Guerrero, H. Shams, I. Fatadin, M. J. Fice, M. Naftaly, A. J. Seeds, and C. C. Renaud, "Single sideband signals for phase noise mitigation in wireless THz-over-fibre systems," *Journal of Lightwave Technology*, vol. 36, no. 19, pp. 4527–4534, 2018. [Online]. Available: <https://ieeexplore.ieee.org/document/8430507/>
- [7] M. Burla, C. Hoessbacher, W. Heni, C. Haffner, Y. Fedoryshyn, D. Werner, T. Watanabe, H. Massler, D. Elder, L. Dalton, and J. Leuthold, "500 GHz Plasmonic Mach-Zehnder Modulator," *APL Photonics*, vol. 4, no. 056106 (2019), pp. 1–11, 2019.
- [8] S. Ummethala, T. Harter, K. Koehnle, Z. Li, S. Muehlbrandt, Y. Kutuvantavida, J. N. Kemal, J. Schaefer, H. Massler, A. Tessmann, S. K. Garlapati, A. Bacher, L. Hahn, M. Walther, T. Zwick, S. Randel, W. Freude, and C. Koos, "Wireless Transmission at 0.3 THz Using Direct THz-to-Optical Conversion at the Receiver," *European Conference on Optical Communication*, no. 1, p. We4.3, 2018.
- [9] C. Wang, J. Yu, X. Li, P. Gou, and W. Zhou, "Fiber-THz-Fiber Link for THz Signal Transmission," *IEEE Photonics Journal*, vol. 10, no. 2, 2018.
- [10] A. Kanno, P. T. Dat, N. Sekine, I. Hosako, N. Yamamoto, Y. Yoshida, K.-i. Kitayama, and T. Kawanishi, "Seamless Fiber-Wireless Bridge in the Millimeter- and Terahertz-Wave Bands," *Journal of Lightwave Technology*, vol. 34, no. 20, pp. 4794–4801, 2016.
- [11] M. F. Hermelo, P.-T. B. Shih, M. Steeg, A. Ngoma, and A. Stöhr, "Spectral efficient 64-QAM-OFDM terahertz communication link," *Optics Express*, vol. 25, no. 16, p. 19360, 2017. [Online]. Available: <https://www.osapublishing.org/abstract.cfm?URI=oe-25-16-19360>
- [12] X. Li, J. Yu, J. Xiao, and Y. Xu, "Fiber-wireless-fiber link for 128-Gb/s PDM-16QAM signal transmission at W-band," *IEEE Photonics Technology Letters*, vol. 26, no. 19, pp. 1948–1951, 2014.
- [13] S. Koenig, J. Antes, D. Lopez-Diaz, R. Schmogrow, T. Zwick, C. Koos, W. Freude, J. Leuthold, and I. Kallfass, "20Gbit/s Wireless Bridge at 220GHz Connecting Two Fiber-Optic Links," *Journal of Optical Communications and Networking*, vol. 6, no. 1, p. 54, 2014. [Online]. Available: <https://www.osapublishing.org/abstract.cfm?URI=jocn-6-1-54>
- [14] S. L. Jansen, I. Morita, T. C. Schenk, N. Takeda, and H. Tanaka, "Coherent optical 25.8-Gb/s OFDM transmission over 4160-km SSMF," *Journal of Lightwave Technology*, vol. 26, no. 1, pp. 6–15, 2008.
- [15] M. Seimetz, "Laser linewidth limitations for optical systems with high-order modulation employing feed forward digital carrier phase estimation," *OFC/NFOEC 2008 - 2008 Conference on Optical Fiber Communication/National Fiber Optic Engineers Conference*, pp. 2–4, 2008.
- [16] L. Gonzalez-Guerrero, H. Shams, I. Fatadin, M. Naftaly, M. J. Fice, C. C. Renaud, and A. J. Seeds, "Comparison of Optical Single Sideband Techniques for THz-Over-Fiber Systems," *IEEE Transactions on Terahertz Science and Technology*, vol. 9, no. 1, pp. 98–105, 2018.
- [17] Y. Zhu, M. Jiang, X. Ruan, C. Li, and F. Zhang, "112Gb / s Single-Sideband PAM4 WDM Transmission over 80km SSMF with Kramers-Kronig Receiver," in *Optical Fiber Communication*, San Diego, 2018.
- [18] D. M. Pozar, *Microwave Engineering*, 4th ed., 2012.
- [19] H. Friis, "Simple Transmission Formula," *Proceedings of the IRE and Waves and Electrons May*, no. 1, pp. 254–256, 1946.
- [20] I. Fatadin, D. Ives, and S. J. Savory, "Differential carrier phase recovery for QPSK optical coherent systems with integrated tunable lasers," *Optics Express*, vol. 21, no. 8, p. 10166, 2013. [Online]. Available: <https://www.osapublishing.org/oe/abstract.cfm?uri=oe-21-8-10166>
- [21] T. Pfau, S. Hoffmann, and R. Noé, "Hardware-efficient coherent digital receiver concept with feedforward carrier recovery for M-QAM constellations," *Journal of Lightwave Technology*, vol. 27, no. 8, pp. 989–999, 2009.
- [22] X. Zhou, "Efficient clock and carrier recovery algorithms for single-carrier coherent optical systems: A systematic review on challenges and recent progress," *IEEE Signal Processing Magazine*, vol. 31, no. 2, pp. 35–45, 2014.
- [23] M. Selmi, Y. Jaouen, and P. Ciblat, "Accurate digital frequency offset estimator for coherent PolMux QAM transmission systems," *2009 35th European Conference on Optical Communication*, no. 1, pp. 3–4, 2009.
- [24] T. Sakamoto, T. Kawanishi, and M. Izutsu, "Widely wavelength-tunable ultra-flat frequency comb generation using conventional dual-drive Mach-Zehnder modulator," *ELECTRONICS LETTERS*, vol. 43, no. 19, 2007.